Cultivation and visualization of a methanogen of the phylum Thermoproteota

Roland Hatzenpichler (rolandhatzenpichler@gmail.com)
Montana State University https://orcid.org/0000-0002-5489-3444
Anthony Kohtz (anthony.kohtz@student.montana.edu)
Montana State University
Viola Krukenberg (viola.krukenberg@montana.edu)
Montana State University
Nickolai Petrosian (nikolai.petrosian@mol.biol.ethz.ch)
ETH Zurich
Zackary Jay (zackary.jay@montana.edu)
Montana State University https://orcid.org/0000-0003-3062-4933
Martin Pilhofer (pilhofer@mol.biol.ethz.ch)
ETH Zurich

Biological Sciences - Article

Keywords:

DOI: https://doi.org/

Additional Declarations: There is **NO** Competing Interest.

Cultivation and visualization of a methanogen of the phylum Thermoproteota

Anthony J. Kohtz[1], Viola Krukenberg[1,#], Nikolai Petrosian[2,#], Zackary J. Jay[1,#], Martin Pilhofer[2], Roland Hatzenpichler[1,3,*]

1, Department of Chemistry and Biochemistry, Center for Biofilm Engineering, and Thermal Biology Institute, Montana State University, Bozeman, MT-59717, USA

2, Institute of Molecular Biology and Biophysics, ETH Zurich, Zurich-8092, Switzerland

3, Department of Microbiology and Cell Biology, Montana State University, Bozeman, MT-59717, USA

#, these authors equally contributed to this work

*, Correspondence to roland.hatzenpichler@montana.edu

Abstract

Methane is the second most abundant climate-active gas and understanding its sources and sinks is a crucial endeavor in microbiology, biogeochemistry, and climate sciences[1,2]. For decades, it was thought that methanogenesis, the ability to conserve energy coupled to methane production, was restricted to a taxonomically and metabolically specialized group of archaea, the Euryarchaeota[1]. The discovery of marker genes for anaerobic alkane cycling in metagenome-assembled genomes obtained from diverse habitats has led to the hypothesis that archaeal lineages outside the Euryarchaeota are involved in methanogenesis[3-6]. Here, we cultured *Candidatus* Methanosuratincola yellowstonensis, a member of the archaeal phylum Thermoproteota, from a terrestrial hot spring. Growth experiments combined with activity assays, stable isotope tracing, and genomic analyses confirmed that this thermophilic archaeon grows via methyl-reducing hydrogenotrophic methanogenesis. Cryo-electron tomography revealed that *Ca*. M. yellowstonensis cells are archaellated coccoid cells that form intercellular bridges that provide two to three cells with a continuous cytoplasm and S-layer. The wide environmental distribution of *Ca*. M. yellowstonensis suggests that they might play important and hitherto overlooked roles in carbon cycling within diverse anoxic habitats.

Introduction

Methanogens, strictly anaerobic archaea that conserve energy coupled to methane production, are responsible for approximately 69% (576 Tg year^{-1}) of global methane emissions[7,8]. Methanogens can exploit CO_2/H_2 and a variety of organic compounds, such as, formate, acetate, or methylated or methoxylated molecules, to fuel their growth[2]. All methanogenic pathways require methyl-coenzyme M reductase (MCR), the enzyme complex catalyzing the conversion of methyl-coenzyme M (CH_3-CoM) and coenzyme B (CoB) into methane and a heterodisulfide (CoM-S-S-CoB)[9]. Because of its crucial importance in all known methanogenic pathways as well as the archaeal anaerobic oxidation of short-chain hydrocarbons, MCR-encoding genes are commonly used to identify potential alkane cycling archaea[2,10].

Methanogens have been cultured since the early 1900s[11] but to date all belong to the superphylum Euryarchaeota, a group that has recently been split into multiple phylum-level lineages[12].

In the last decade, the discovery of *mcr* and other methanogenesis marker genes in metagenome-assembled genomes (MAGs) has led to the proposal that several lineages within the archaeal phyla Asgardarchaeota, Hadarchaeota, and Thermoproteota (formerly the TACK superphylum) might also engage in anaerobic alkane cycling[3-6,13,14]. In contrast to most cultured methanogens that conserve energy exclusively via methanogenesis, many of these MCR-encoding MAGs encode additional growth strategies, such as dissimilatory sulfite reduction[3,14] or fermentation[5,6]. The potential of these MCR-encoding archaea to switch their growth modality depending on environmental conditions might provide them an advantage over obligate methanogens. However, so far, no methanogen from outside the Euryarchaeota has been cultured or even visualized by microscopy, and there is no experimental evidence to support metagenome-based predictions of their metabolism. Geothermal features, such as hot springs, have recently been shown to harbor a wide diversity of MCR-encoding archaea[3,4,14-17]. The extreme nature of hot springs reduces their community complexity relative to temperate environments, which makes them promising sources for targeted cultivation of these microorganisms.

Here we combined cultivation, microscopy, metagenomics, growth experiments, stable isotope tracing, and single cell activity assays to demonstrate that a member of the phylum Thermoproteota is a methyl-reducing hydrogenotrophic methanogen. We for the first time visualize a methanogen outside the Euryarchaeota and its unique ultrastructure by fluorescence microscopy and cryo-electron tomography (CryoET).

Cultivation of a novel methanogen

In a recent survey of 100 geothermal features in Yellowstone National Park (YNP), we identified the Lower Culex Basin (LCB) as an area with strong potential for anaerobic methane cycling[16]. From sediments of one of these hot springs, designated feature LCB070, we obtained a metagenome from which we reconstructed several MCR-encoding MAGs. Based on phylogenomic analysis two MAGs affiliated with the Verstraetearchaeota[6] (a.k.a. Methanomethylicia[12]), a lineage that is now proposed as part of the phylum Thermoproteota[12] (formerly the TACK superphylum; Extended Data Fig. 1), were recovered. Based on our genomic analysis, the two MAGs, as well as related MAGs previously obtained from other samples[3,6,17,18], encode the potential for methyl-reducing hydrogenotrophic methanogenesis.

Using a sediment slurry from hot spring LCB070 as inoculum, we initiated a methanogenic culture that was supplied with methanol and H_2 and incubated in anoxic media (64ºC, pH 6.5). After one transfer of the culture, fluorescence *in situ* hybridization (FISH) with a newly designed Methanomethyliaceae-specific 16S rRNA-targeted oligonucleotide probe revealed an abundant population of coccoid cells. We selected this methanogenic enrichment for metagenomic sequencing, which revealed that the most abundant organism was a member of

the Verstraetearchaeota (31.4% relative abundance). After multiple transfers into fresh media, we obtained a sediment-free and methanogenic culture consistently enriched in this archaeon.

Via a combination of Illumina short-read and Nanopore long-read sequencing, we recovered the complete circular genome of this archaeon. The reconstructed genome has a size of 1.52 Mb and a GC content of 54.6%. 16S rRNA gene and single copy marker protein phylogenies placed the archaeon within the phylum Thermoproteota (Fig. 1A). Comparative amino acid, nucleotide, and 16S rRNA gene sequence identity analyses further classified the genome within the genus *Ca*. Methanosuratincola[6,19] (Extended Data Fig. 2 and 3). We propose to name this archaeon *Ca.* Methanosuratincola yellowstonensis strain LCB70. Interestingly, strain LCB70 was not closely related to the two MAGs recovered from the original hot spring metagenome (Extended Data Fig 1 and 2), suggesting that it represented a low abundance population in feature LCB070 at the time of sampling.

By the seventh transfer the only archaeal populations detectable by 16S rRNA gene amplicon sequencing were strain LCB70 (32.8% relative abundance) and *Methanothermobacter* spp. (9.7% relative abundance) (Fig. 1B). In FISH experiments with LCB70-specific and general archaeal probes, we were able to distinguish their cells by coccoid (LCB70) and filamentous (*Methanothermobacter* spp.) morphologies (Fig. 1C). Thus, we established a stable mixed culture of LCB70, a proposed methyl-reducing methanogen, and *Methanothermobacter* spp., obligate CO_2-reducing methanogens.

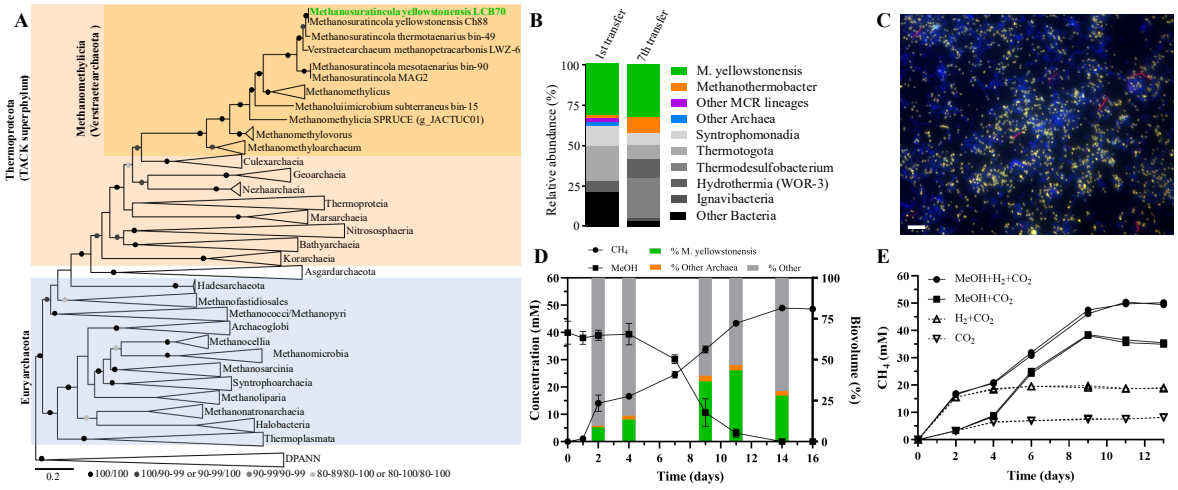

Figure 1. Characterization of the methanogenic enrichment culture. A. Phylogenomic tree of archaea, built with a set of 33 single copy marker genes, with *Ca.* M. yellowstonensis strain LCB70 highlighted in green. **B.** Community composition of the culture. Left, relative abundance of strain LCB70 genome and MAGs recovered from metagenome sequencing of the 1st transfer. Right, 16S rRNA gene amplicon sequencing of the 7th transfer. **C.** Visualization of the enrichment culture by 16S rRNA-targeted FISH. LCB70 cells in yellow (labeled by the Methanomethyliaceae-specific probe Msur657 and the general archaeal probe Arch915), other archaeal cells in red (labeled by Arch915 only). DAPI-stained cells not hybridizing with either probe are in blue. Scale bar, 5 µm. **D.** Growth curve depicting methane production, methanol depletion, and relative abundance of strain LCB70 and other archaea (%) over time, demonstrating the increase of *Ca.* M. yellowstonensis LCB70 from 8.7% in the lag-phase to 43.5% in log phase of methane production. Data for methane and methanol (MeOH) are the mean ± s.d. and % biovolume is the mean of four biological replicates. **E.** Methane production by the culture under different

substrate amendments. Data for two biological replicates are shown. Methane production in incubations with carbon dioxide with or without hydrogen is due to the activity of *Methanothermobacter*. When methanol, a substrate that *Methanothermobacter* cannot use, is present strain LCB70 converts it into methane via methyl-reducing methanogenesis.

Strain LCB70 converts methanol to methane

In cultures supplied with methanol and H_2 the abundance of strain LCB70 increased alongside methane production and methanol depletion (Fig. 1D). The biovolume fraction of LCB70 in the culture over time was analyzed with FISH, exhibiting an increase from an average of 8.7% in the lag phase to up to 43.5% during the log phase of methane production and methanol depletion (Fig. 1D). In the stationary phase, when methanol was fully depleted and methane production ceased, the LCB70 biovolume fraction decreased to 28%, likely due to methanol starvation or potential viral predation (Fig. 1D; virus-like particles were observed via CryoET, see below). When methanol was omitted from the culture, methane production was strongly reduced and growth of LCB70 could not be sustained (Fig. 1E). According to FISH, the biovolume of *Methanothermobacter* in our culture ranged from an average of 0.9% by day 2 to 3.4% by day 11 (Fig. 1D). In the first two days of the culture, methane production is not coupled to methanol depletion and LCB70 is of comparatively low abundance. In contrast, during later stages of the culture, when methane production is coupled to methanol depletion, LCB70 is most abundant, further indicating the reliance of LCB70 on methanol (Fig. 1D).

To gain insight into the metabolic activity of strain LCB70 under methanogenic and non-methanogenic conditions, we performed bioorthogonal non-canonical amino acid tagging (BONCAT) incubations to label translationally active cells[20,21]. We grew replicate cultures and during the exponential phase of methane production spiked 2-bromoethanesulfonate (BES), an inhibitor of the MCR complex, into one set of cultures. After a 48-hour incubation with or without BES, we added *L*-homopropargylglycine (HPG) as a tracer of translational activity to all cultures. After a 24-hour incubation under these conditions we analyzed cells from the incubations by BONCAT-FISH to directly link identity and translational activity at a single cell level. We observed activity of LCB70 cells under methanogenic conditions (absence of BES). In contrast, LCB70 abundance and activity strongly decreased when methane production stopped upon BES addition (Fig. 2A,B). This suggests that LCB70 is reliant on the activity of the MCR complex for energy conservation, and subsequent translational activity, via methanogenesis.

When H_2 was not supplied, methane production still occurred, which indicated other members of the culture are likely responsible for H_2 production (Fig. 1E). We conducted a stable isotope labeling experiment, in which a culture grown in the absence of H_2 was incubated in the presence of ^{13}C-methanol. We observed that 52% of the added ^{13}C-methanol was converted to ^{13}C-methane and that 40% was converted to ^{13}C-carbon dioxide (Fig. 2C). While both strain LCB70 and *Methanothermobacter* populations were present in the culture, they drastically differ in their methanogenesis pathways. LCB70 encodes genes for methyl-reducing methanogenesis but lacks the genes for CO_2-reducing hydrogenotrophic methanogenesis. In contrast, the *Methanothermobacter* spp. in our enrichment as well as the two

Methanothermobacter strains that had previously been cultured from other Yellowstone hot springs[22,23] lack methyltransferase genes and are strictly limited to H_2 and CO_2 for methane production. The production of ^{13}C-carbon dioxide suggests that other organisms in the enrichment culture also metabolize methanol. Consistent with this idea, populations affiliated with the bacterial lineages Syntrophomonadia (7-12% relative abundance) and Thermotogota (8-21% relative abundance) are abundant in our enrichment (Fig. 1B; Supplementary Table 1) and encode methanol methyltransferases (MtaABC) and methanol dehydrogenases, respectively. They may use these enzymes to oxidize methanol to carbon dioxide. We hypothesize that these methanol-degrading bacteria in the culture likely form H_2 and acetate in addition to carbon dioxide, and engage in a syntrophic interaction with H_2-consumers, *i.e.* strain LCB70 and *Methanothermobacter*. This type of metabolic interaction has been reported for other thermophilic, methanogenic co-cultures and bioreactors[24,25]. In future studies, ^{13}C- and ^{2}H-labeling experiments performed under different physicochemical conditions might help to reconcile these ideas.

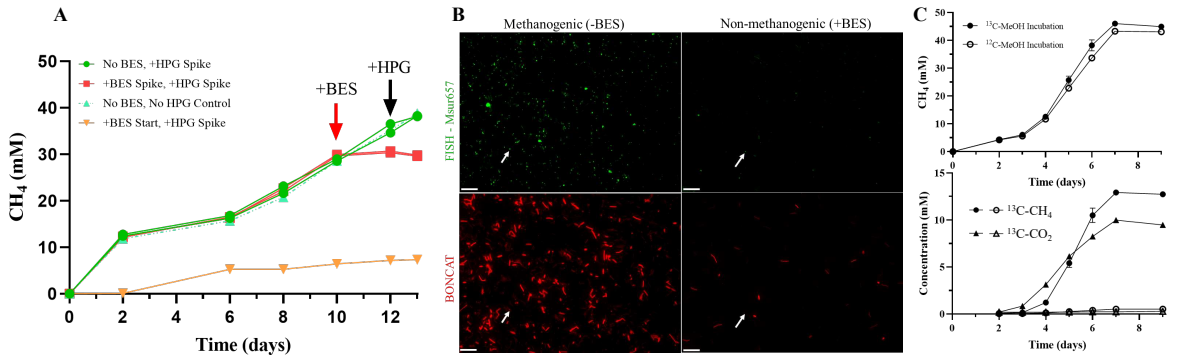

Figure 2. Activity of strain LCB70 and conversion of stable isotope tracers by the culture. A. Methane production over time during the BONCAT-FISH experiment. Arrows indicate BES (red) and HPG (green) addition. BES addition on day 10 stops methane production. **B.** LCB70 cells detected via FISH (green) and translationally active cells detected via BONCAT (red). Under methanogenic conditions, LCB70 cells were translationally active. When methanogenesis was inhibited by BES, LCB70 cells became inactive. White arrows indicate examples of LCB70 cells. Note that the relative fluorescence intensity of LCB70 as compared to other cells is non-informative in BONCAT-experiments[21]. **C.** Incubation experiments with ^{13}C-methanol (25 mM ^{13}C-methanol and 25 mM ^{12}C-methanol were added; closed symbols) and ^{12}C-methanol (50 mM added) as control (open symbols). Top, total methane produced over the incubation. Bottom, ^{13}C-methane (circles) and ^{13}C-carbon dioxide (triangles) produced by the cultures.

Metabolic potential of strain LCB70

With the recovery of the complete circular genome of LCB70, we reconstructed the metabolic potential of this organism. Consistent with the observation of methane production from methanol in culture, LCB70 encodes the potential for methyl-reducing methanogenesis by using methanol and H_2. Encoded methanol-specific methyltransferases (MtaABC) transfer the methyl group of methanol, forming CH_3-CoM, which can then be converted to CoM-S-S-CoB and methane by the MCR complex (Fig. 3 A,B). LCB70 also encodes several other methyltransferases that could be involved in converting other methylated substrates, such as

methylamines, to methane. However, attempts to grow the culture on methylamines have so far been unsuccessful. Furthermore, LCB70 lacks the tetrahydromethanopterin S-methyltransferase (MTR) complex and methyl branch of the Wood-Ljungdahl pathway, indicating it is not able to oxidize methanol to CO_2, which would be required for a methyl-dismutating methanogenesis pathway[2].

LCB70 encodes several complexes that could be involved in the reduction of CoM-S-S-CoB, energy conservation, and hydrogen metabolism. We found genes encoding heterodisulfide reductase (HdrBC) adjacent to genes of the proposed [NiFe]-hydrogenase complex, Ehd, which could couple the oxidation of H_2 to the reduction of CoM-S-S-CoB and translocation of H^+ or Na^+ ions across the membrane[3,26]. A group 4i [NiFe]-hydrogenase, Ehb, is also encoded in the LCB70 genome. In other methanogens, Ehb has been implicated in several processes, including energy conservation and H_2 production in *Methanosphaera stadtmanae*, and providing reduced ferredoxins for anabolic processes in *Methanococcus maripaludis*[1,27]. Thus, the function and regulation of Ehb in LCB70 is unclear and will require additional physiology studies to deduce the role(s) of this hydrogenase in the metabolism of LCB70. Additionally, a cytoplasmic group 3b [NiFe]-hydrogenase is encoded. This group of potential sulfhydrogenases catalyzes the reversible oxidation of NADPH coupled to the reduction of protons or sulfur (S^0) to H_2 or H_2S[28].

Notably, in contrast to previous findings based on Verstraetearchaeota MAGs[6,17], we did not find an Fpo-like complex in the LCB70 genome. However, we found a novel group 4g [NiFe] hydrogenase, termed Ehi here, encoded in LCB70 and other diverse Thermoproteota lineages, and that shares similarities to Fpo-like complexes in archaea (Fig. 3C). This Ehi complex has the same 11-subunit organization found in Fpo complexes. However, the catalytic subunit has conserved motifs (CxxC) at the N and C-terminus, for coordination of a [NiFe] cofactor, which are absent in Fpo/Nuo complexes[29,30]. Therefore, we suggest Ehi could functionally substitute for a Fpo-like complex in LCB70. If Ehi forms a complex with HdrD, in a similar fashion to the Fpo/HdrD complex in Methanomassiliicoccales[29], it might constitute another group of potential heterodisulfide reductase associated hydrogenases (Fig. 3A). Alternatively, if Ehi does not form a complex with HdrD, it would be functionally more similar to the Ehb-type hydrogenase.

In LCB70, as in the first description of Verstraetearchaeota MAGs[6], a gene with similarity to lactate dehydrogenase (GlcD) was present and co-located with a heterodisulfide reductase (HdrD) gene[6]. Additionally, we identified a second cluster of genes with two additional HdrD copies that are next to a gene containing a lactate utilization domain (LUD)[31] and a [4Fe-4S] dicluster domain (Fig. 3A; LldG-like; Extended Data Fig. 4). Prior analyses of Verstraetearchaeota MAGs identified GlcD-like, but not LldG-like genes. As suggested previously[6,10,17] these genes may enable lactate to be used as an electron donor to a Ehi/HdrD complex for the reduction of CoM-S-S-CoB, a property that has not been observed in any cultured Euryarchaeal methanogens.

Lactate has been observed to be metabolized in syntrophic co-cultures, in which H_2 produced by lactate fermentation can be used by H_2-consuming methanogens[32,33]. However, the potential for direct use as an electron donor in CoM-S-S-CoB reduction presents some unique metabolic

scenarios for LCB70. Lactate is a common byproduct of fermentative organisms and, in competition for H_2, it could serve as an alternative or additional electron donor for methanogenesis by LCB70. Downstream reductive metabolism of pyruvate could provide a carbon source, or pyruvate could be further oxidized to acetyl-CoA and reduced ferredoxin by pyruvate:ferredoxin oxidoreductase. Acetyl-CoA synthetase could then convert acetyl-CoA to acetate and ATP. The connection between lactate and methanogenesis will need to be studied further to understand how these processes might affect the metabolism of LCB70. In summary, the reconstruction of the methane and energy conservation pathways of LCB70 is consistent with methyl-reducing hydrogenotrophic methanogenesis from methanol.

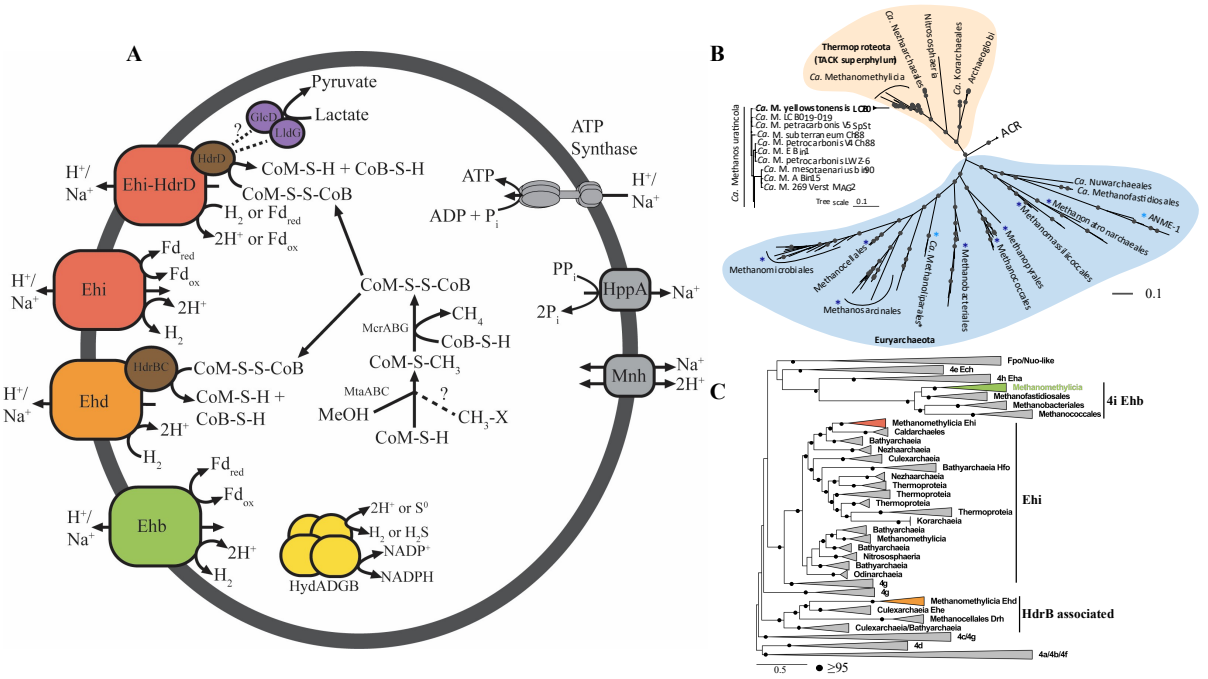

Figure 3. Proposed methane and hydrogen metabolism in strain LCB70. A. Metabolic reconstruction of methyl-reducing methanogenesis and energy conservation pathways in LCB70. A list of genes used to construct this figure can be found in Supplementary Table 2. **B.** Phylogenetic tree of McrA sequences demonstrating the affiliation of LCB70 McrA within the Methanomethylicia (Thermoproteota; tan shading). Asterisks indicate lineages with isolates (dark blue) or enrichments (light blue) within the Euryarchaeota (blue shading), circles indicate bootstrap support >98%. **C.** Phylogenetic tree of group 4 [NiFe]-hydrogenases. The colors for the Ehb, Ehd, and Ehi clades match those in A.

Ultrastructure of strain LCB70

Cultivation of strain LCB70 allowed us, for the first time, to study the ultrastructure of a methanogen outside the Euryarchaeota. We imaged plunge-frozen cells of an active LCB70 culture via cryo-electron tomography (CryoET). According to FISH, LCB70 cells were the only coccoid archaeal cells in the enrichment (Fig. 1C). Their unique shape, high relative abundance, and presence of a S-layer enabled their identification in tomograms. LCB70 cells were surrounded by a cytoplasmic membrane and an S-layer and had an average diameter of 845 ± 163 nm (n = 56 cells; Fig. 4, Extended Data Fig. 5). The observation of chemotaxis arrays and archaella indicates that LCB70 cells are motile and capable of sensing and

responding to environmental stimuli[34]. Other structures observed on and inside LCB70 cells include filamentous and spindle shaped virus-like particles (Fig. 4, Extended Data Fig. 5) and unidentified intracellular semi-ordered filamentous structures and putative storage granules (Fig. 4 A,B, Extended Data Fig. 5, Supplementary Movie 1).

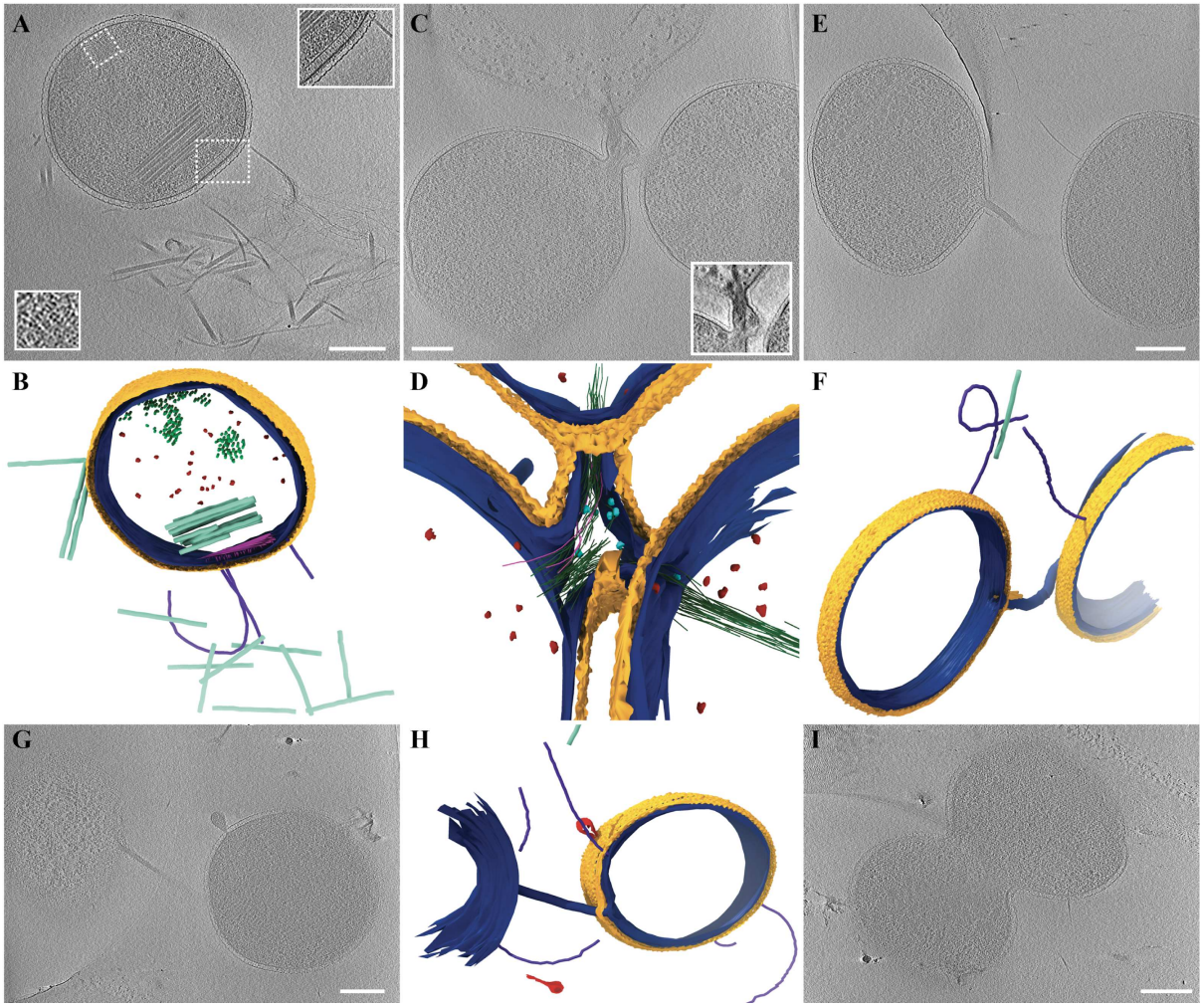

Figure 4. Cryo-electron tomography of LCB70 cells. Their unique shape, high abundance, and S-layer enabled the unambiguous identification of strain LCB70 cells in tomograms. **A, B.** Tomographic slice and corresponding model of a LCB70 cell. The S-layer is shown in yellow, the cytoplasmic membrane in blue, putative ribosomes in red, archaella in purple, viruses in cyan, chemotaxis receptor arrays in pink, and unidentified filamentous structures in green. Insets in A show magnified views of the latter two features. **C, D.** Tomographic slice and corresponding model of a three-way cell junction (inset in C shows higher contrast image) with a continuous cytoplasmic membrane and S-layer that connects three cells. Ribosomes (red), putative ribosomes (cyan), and unidentified filaments are located inside the cell junction. Some of these filaments are contained within the volume connecting the three cells (green), while others span from one cell to another (pink). **E, F.** Tomographic slice and corresponding model of two LCB70 cells connected by a cell-cell bridge that is only partially covered by an S-layer. **G, H**. Tomographic slice and corresponding model of a cell-cell bridge without surrounding S-layer. Structures in red are interpreted to either represent spindle-shaped viruses or early protrusions of the cell membrane that would eventually develop into cell-cell bridges. **I**. An example of a dividing LCB70 cell. All scale bars equal 200 nm. For additional tomograms see Extended Data Figures 5 and 7, and Supplementary Movie 1.

During FISH analyses we observed LCB70 cells to sometimes form aggregates (Fig. 1C and Extended Data Fig. 6), suggesting that these archaea might be able to form direct cell-cell interactions. Indeed, via cryoET we observed cell-cell bridges with a continuous cytoplasmic membrane and in some cases a continuous S-layer between LCB70 cells (Fig. 4, Extended Data Fig 7). We only observed cell-cell bridges between LCB70 cells, suggesting that either these interactions are LCB70-specific or that direct cellular connections between LCB70 and other cells are rare. We also visualized structures with larger compartments along these cell-cell bridges, which resembled vesicles, as well as cellular connections without a surrounding S-layer (Fig. 4, Extended Data Fig. 7). We interpret these structures to be intermediate forms of the same cell-cell bridges surrounded by an S-layer that connect LCB70 cells. In one tomogram, the volume of a cell-cell bridge (120-140 nm inner diameter, 160-220 nm outer diameter) shared by three cells contained both putative ribosomes and filaments of unknown composition (Fig. 4 C,D). At this point, we can only speculate about the nature of these interactions and how they form.

In bacteria, cell-cell bridges, including nanotubes, have been shown to be involved in diverse intra- and inter-species interactions, including the exchange of metabolites, electrons, and DNA[35]. While their function in archaea is not well understood, cell-cell bridges and other cell-cell connections have been observed in at least three different archaeal phyla[36]. Cell-cell bridges of strain LCB70 cells (29-38 nm inner diameter; 71-73 nm outer diameter) most closely resemble those observed in *Haloferax volcanii* (57-162 nm outer diameter). Like for LCB070, *H. volcanii* nanotubes are covered by a continuous S-layer and occasionally contain ribosomes and filaments of unknown composition that are speculated to enable cytoplasmic exchange between cells[37].

Conclusions

In summary, we provide experimental and genomic evidence for methyl-reducing hydrogenotrophic methanogenesis by *Ca*. Methanosuratincola yellowstonensis strain LCB70 through enrichment cultivation, growth experiments, single cell activity measurements, conversion of isotopically labeled methanol, and metabolic reconstructions. Additionally, we provide a first look into the ultrastructure of this species, revealing structures related to motility and cell-cell connections that may enable exchange of cytoplasmic material. Analysis of *Ca*. Methanosuratincola related 16S rRNA gene sequences in public databases revealed that these archaea are present in a variety of anoxic habitats, including bioreactors, hot springs, rumen, sediments, soils, and wastewater (Extended Data Fig. 8). Thus, *Ca*. M. yellowstonensis likely contribute to anaerobic carbon cycling dynamics in both natural and engineered environments. Future culture-dependent studies of *Ca*. M. yellowstonensis will focus on the biochemistry and regulation of methanogenesis as well as structural and functional aspects of their cell biology.

Etymology

LCB70 is a methanogen affiliated with the phylum Thermoproteota within the candidate genus *Methanosuratincola*[6,19] for which we propose the name *Ca.* Methanosuratincola yellowstonensis sp. nov.

Me.tha.no.su.rat.in'co.la. N.L. pref. *methano-* pertaining to methane; L. masc. or fem. n. *incola*, inhabitant; N.L. masc. n. *Methanosuratincola*, methanogen inhabiting the Surat Basin, where this lineage was discovered via metagenomics[6]. yel.low.ston.en'sis N.L. masc. adj. *yellowstonensis*, from Yellowstone.

Locality. Sediment from a hot spring, identified as feature LCB070 in a recent survey[16] of Yellowstone National Park (WY, USA) geothermal features.

Diagnosis. A thermophilic methyl-reducing hydrogenotrophic methanogen of the phylum Thermoproteota that grows as coccoid cells with a diameter of 845 ± 163 nm. Its genome has a length of 1.52 Mb and a GC content of 54.6%.

For a protologue, please see the supplementary online information.

Online content

Any methods, additional references, Nature Research reporting summaries, source data, extended data, supplementary information, acknowledgements, details of author contributions and competing interests, as well as statements of data and code availability will be available as supplementary online information.

References

1 Thauer, R. K., Kaster, A.-K., Seedorf, H., Buckel, W. & Hedderich, R. Methanogenic archaea: ecologically relevant differences in energy conservation. *Nature Reviews Microbiology* **6**, 579-591 (2008).

2 Garcia, P. S., Gribaldo, S. & Borrel, G. Diversity and Evolution of Methane-Related Pathways in Archaea. *Annu Rev Microbiol* **76**, 727-755, doi:10.1146/annurev-micro-041020-024935 (2022).

3 Borrel, G. *et al.* Wide diversity of methane and short-chain alkane metabolisms in uncultured archaea. *Nat Microbiol* **4**, 603-613, doi:10.1038/s41564-019-0363-3 (2019).

4 Wang, Y., Wegener, G., Hou, J., Wang, F. & Xiao, X. Expanding anaerobic alkane metabolism in the domain of Archaea. *Nature microbiology* **4**, 595-602 (2019).

5 Evans, P. N. *et al.* Methane metabolism in the archaeal phylum Bathyarchaeota revealed by genome-centric metagenomics. *Science* **350**, 434-438 (2015).

6 Vanwonterghem, I. *et al.* Methylotrophic methanogenesis discovered in the archaeal phylum Verstraetearchaeota. *Nature microbiology* **1**, 1-9 (2016).

7 Saunois, M. *et al.* The Global Methane Budget 2000-2017. *Earth Syst Sci Data* **12**, 1561-1623, doi:10.5194/essd-12-1561-2020 (2020).

8 Conrad, R. The global methane cycle: recent advances in understanding the microbial processes involved. *Environ Microbiol Rep* **1**, 285-292, doi:10.1111/j.1758-2229.2009.00038.x (2009).
9 Thauer, R. K. Methyl (Alkyl)-Coenzyme M Reductases: Nickel F-430-Containing Enzymes Involved in Anaerobic Methane Formation and in Anaerobic Oxidation of Methane or of Short Chain Alkanes. *Biochemistry* **58**, 5198-5220, doi:10.1021/acs.biochem.9b00164 (2019).
10 Evans, P. N. *et al.* An evolving view of methane metabolism in the Archaea. *Nat Rev Microbiol* **17**, 219-232 (2019).
11 Stephenson, M. & Stickland, L. H. Hydrogenase: The bacterial formation of methane by the reduction of one-carbon compounds by molecular hydrogen. *Biochem J* **27**, 1517-1527, doi:10.1042/bj0271517 (1933).
12 Rinke, C. *et al.* A standardized archaeal taxonomy for the Genome Taxonomy Database. *Nature Microbiology* **6**, 946-959 (2021).
13 Seitz, K. W. *et al.* Asgard archaea capable of anaerobic hydrocarbon cycling. *Nature Communications* **10**, doi:10.1038/s41467-019-09364-x (2019).
14 McKay, L. J. *et al.* Co-occurring genomic capacity for anaerobic methane metabolism and dissimilatory sulfite reduction discovered in the *Korarchaeota*. *Nat Microbiol* **4**, 614-622 (2019).
15 McKay, L. J., Hatzenpichler, R., Inskeep, W. P. & Fields, M. W. Occurrence and expression of novel methyl-coenzyme M reductase gene (*mcrA*) variants in hot spring sediments. *Sci Rep* **7**, DOI:10.1038/s41598-41017-07354-x (2017).
16 Lynes, M. *et al.* Diversity and function of methyl-coenzyme M reductase-encoding archaea in Yellowstone hot springs revealed by metagenomics and mesocosm experiments. *BioRxiv*, doi: https://doi.org/10.1101/2022.08.18.504445 (2022).
17 Hua, Z.-S. *et al.* Insights into the ecological roles and evolution of methyl-coenzyme M reductase-containing hot spring Archaea. *Nature communications* **10**, 1-11 (2019).
18 Liu, Y.-F. *et al.* Long-term cultivation and meta-omics reveal methylotrophic methanogenesis in hydrocarbon-impacted habitats. *Engineering* (2022).
19 Oren, A., Garrity, G. M., Parker, C. T., Chuvochina, M. & Trujillo, M. E. Lists of names of prokaryotic Candidatus taxa. *International Journal of Systematic and Evolutionary Microbiology* **70**, 3956-4042 (2020).
20 Hatzenpichler, R. *et al.* Visualizing in situ translational activity for identifying and sorting slow-growing archaeal− bacterial consortia. *Proceedings of the National Academy of Sciences* **113**, E4069-E4078 (2016).
21 Hatzenpichler, R., Krukenberg, V., Spietz, R. L. & Jay, Z. J. Next-generation physiology approaches to study microbiome function at single cell level. *Nature Reviews Microbiology*, 1-16 (2020).
22 Zeikus, J., Ben-Bassat, A. & Hegge, P. Microbiology of methanogenesis in thermal, volcanic environments. *Journal of Bacteriology* **143**, 432-440 (1980).
23 McKay, L. J., Klingelsmith, K. B., Deutschbauer, A. M., Inskeep, W. P. & Fields, M. W. Draft genome sequence of Methanothermobacter thermautotrophicus WHS, a thermophilic hydrogenotrophic methanogen from Washburn Hot Springs in Yellowstone National Park, USA. *Microbiology resource announcements* **10**, e01157-01120 (2021).

24 Balk, M., Weijma, J. & Stams, A. J. Thermotoga lettingae sp. nov., a novel thermophilic, methanol-degrading bacterium isolated from a thermophilic anaerobic reactor. *International Journal of Systematic and Evolutionary Microbiology* **52**, 1361-1368 (2002).
25 Paulo, P. *et al.* Pathways of methanol conversion in a thermophilic anaerobic (55 C) sludge consortium. *Applied microbiology and biotechnology* **63**, 307-314 (2003).
26 Kohtz, A. J., Jay, Z. J., Lynes, M. M., Krukenberg, V. & Hatzenpichler, R. Culexarchaeia, a novel archaeal class of anaerobic generalists inhabiting geothermal environments. *ISME Communications* **2**, 1-13 (2022).
27 Major, T. A., Liu, Y. & Whitman, W. B. Characterization of energy-conserving hydrogenase B in Methanococcus maripaludis. *Journal of bacteriology* **192**, 4022-4030 (2010).
28 Lang, K. *et al.* New mode of energy metabolism in the seventh order of methanogens as revealed by comparative genome analysis of "Candidatus Methanoplasma termitum". *Appl. Environ. Microbiol.* **81**, 1338-1352 (2015).
29 Loh, H. Q., Hervé, V. & Brune, A. Metabolic potential for reductive acetogenesis and a novel energy-converting [NiFe] hydrogenase in Bathyarchaeia from termite guts–A genome-centric analysis. *Frontiers in microbiology* **11**, 635786 (2021).
30 Hwang, W. C. *et al.* LUD, a new protein domain associated with lactate utilization. *BMC bioinformatics* **14**, 1-9 (2013).
31 Bryant, M., Campbell, L. L., Reddy, C. & Crabill, M. Growth of Desulfovibrio in lactate or ethanol media low in sulfate in association with H2-utilizing methanogenic bacteria. *Applied and environmental microbiology* **33**, 1162-1169 (1977).
32 McInerney, M. J. & Bryant, M. P. Anaerobic degradation of lactate by syntrophic associations of Methanosarcina barkeri and Desulfovibrio species and effect of H2 on acetate degradation. *Applied and Environmental Microbiology* **41**, 346-354 (1981).
33 Briegel, A. *et al.* Structural conservation of chemotaxis machinery across A rchaea and B acteria. *Environmental microbiology reports* **7**, 414-419 (2015).
34 Baidya, A. K., Bhattacharya, S., Dubey, G. P., Mamou, G. & Ben-Yehuda, S. Bacterial nanotubes: a conduit for intercellular molecular trade. *Current opinion in microbiology* **42**, 1-6 (2018).
35 Liu, J. *et al.* Extracellular membrane vesicles and nanotubes in Archaea. *microLife* **2** (2021).
36 Sivabalasarma, S. *et al.* Analysis of Cell–Cell Bridges in Haloferax volcanii Using Electron Cryo-Tomography Reveal a Continuous Cytoplasm and S-Layer. *Frontiers in microbiology* **11**, 612239 (2021).

Methods

Chemicals

Unless otherwise specified, all chemicals were obtained from Sigma.

Source of inoculum and cultivation

Sediments from hot spring LCB070 (44°34'01.8"N 110°48'20.2"W) located in the Lower Culex Basin (LCB) thermal complex of Yellowstone National Park, WY, USA (YNP) were obtained in October 2019. A mixture of surface sediments (~1 cm deep) and water (62 °C, pH 8.2) were collected into a sterile glass bottle that was sealed with a thick butyl-rubber stopper without headspace. After transport to the lab, sediments were stored at room temperature. Enrichment cultures were established using anoxic medium containing a base of (per liter): KH_2PO_4, 0.5 g; $MgSO_4 \cdot 7H_2O$, 0.4 g; NaCl, 0.5 g; NH_4Cl, 0.4 g; $CaCl_2 \cdot 2H_2O$, 0.05 g; 2-N-morpholino-ethanesulfonic acid (MES), 2.17 g; yeast extract, 0.1 g; and 0.002% (w/v) $(NH_4)_2Fe(SO_4)_2 \cdot 6H_2O$, 5 mM $NaHCO_3$, 1 mL trace element solution SL-10, 1 mL Selenite-Tungstate solution, 1 mL CCM vitamins[38], 0.0005% (w/v) resazurin, 10 mg of coenzyme-M, 2 mg sodium dithionite, 1 mM dithiothreitol, 1 mM $Na_2S \cdot 9H_2O$. The pH was adjusted to 6.5. Sediment slurry was added (10% v/v) and vials were sealed with thick butyl-rubber stoppers and aluminum crimps in an anoxic glove box (Coy). The headspace of the enrichments was sparged with N_2:CO_2 (90:10) for 5 minutes and set to 200 kPa. Methanol (MeOH) and H_2 were added to a final concentration of 10 mM and 50%, respectively. The cultures were incubated at 64 °C in the dark without shaking. Batch cultures were maintained by transfer of 10% v/v inoculum into fresh medium. A sediment-free culture was obtained after three transfers, after which the culture was maintained on increased MeOH concentrations of 40-50 mM and the addition of 10 mM sodium *L*-lactate as an additional carbon source. Replicate cultures for comparing methane production with or without H_2 and MeOH were performed in duplicate in 30 mL incubation volumes in a 60 mL serum bottle.

Fluorescence in situ hybridization and biovolume calculation

Subsamples were chemically fixed with paraformaldehyde (PFA, 2% final concentration) for 1 hour at room temperature, washed, and stored in 1x phosphate buffered saline (PBS) at 4°C. An oligonucleotide probe targeting most Methanomethyliciaceae 16S rRNA sequence contained in the Silva[39] database (version 132) was designed using the probe design tool in ARB[40] (Msur657, 5'-CCCTCAACCTCTCCCGCC-3'). According to TestProbe[39] using the Silva138 database, this probe detects 71% of 16S rRNA sequences within the family Methanomethyliaceae, and only binds two non-target sequences outside that group. Both sequences are found in the Geoarchaeales, which are absent from our enrichment culture. DOPE-FISH was performed according to Stoecker *et al.* 2010[41] using the Msur657 probe doubly labeled with FAM (obtained from IDT-DNA). In order to track *Ca.* Methanosuratincola yellowstonensis LCB70 and other archaeal cells, a general archaea-targeted probe Arch915[42], double labeled with Alexa Fluor 647, was used in combination with the FAM-labeled Msur657 probe and the DNA-stain 4′,6-diamidino-2-phenylindole (DAPI). All hybridization reactions were carried out at a formamide concentration of 35% (Supplementary Table 4). Negative

controls employed double-labeled NONEUB338[43] and were performed in parallel at a formamide concentration of 35%.

Because the enrichment contained cell aggregates that could not be disassociated (*e.g.*, by sonication or detergent addition) quantitative FISH on a per-cell basis was not possible. Instead, biovolume fractions of LCB70 (cells that bound Msur657 and Arch915) and other archaea (cells that bound to Arch915) in the culture was performed according to Daims 2009[44]. Briefly, PFA-fixed biomass was applied to a slide and DOPE-FISH was performed with the Msur657 and Arch915 as described above, followed by counter-staining with DAPI and embedding in Citifluor. Cells were imaged with a Leica DM4B epifluorescence microscope. Images were segmented and biovolumes calculated with the daime software package[45].

DNA extraction and metagenome sequencing

Hot spring sediment from site LCB070 was collected in October 2019 using a sterile metal cup and was immediately frozen in a dry ice-ethanol bath. DNA was extracted from 10 mL of sediment following the protocol by Zhou *et al*. 1996[46]. Truseq libraries were prepared and sequenced at the DOE Joint Genome Institute (JGI) on the Illumina NovaSeq S4 platform following a 2 x 150 bp indexed run recipe.

15 mL of the first transfer of the LCB070 culture was collected under anoxic conditions and centrifuged at 16,000 x g for 5 minutes to pellet cells, the supernatant was removed, and the pellet stored at -80 °C. Genomic DNA was extracted from the cell pellet using the protocol by Zhou *et al.*[46], with the following modifications. The proteinase K step was extended to 1 hour and the precipitation was performed in the presence of 0.7x volumes isopropanol and 0.1x volume of 3M sodium acetate. Crude extracts were purified using a Zymo clean and concentrator kit (DCC-10, Zymo Research) according to the manufacturer's instructions. Purified genomic DNA was shipped to the Michigan State University genomics core for library preparation and sequencing. A metagenomic library was constructed with the TruSeq Nano DNA kit according to the manufacturer's recommendations. The library was sequenced on an Illumina NovaSeq 6000 platform using the NovaSeq XP reagent kits, SP flow cell, and followed a 2 x 150 bp indexed run recipe.

Nanopore long-read sequencing was performed using a MinION platform and a R9.4.1 flow cell (Oxford Nanopore Technologies). Library preparation was performed using the rapid kit (SQK-RBK004) according to the manufacturer's instructions. Flow cells were run for 72 hours, resulting in 1.3 Gbp of total sequence data. Base-calling was performed with Guppy (v5.0.16+b9fcd7b) using model dna_r9.4.1_450bps_hac and parameters, --trim_barcodes, --detect_mid_strand_adapter, and --detect_mid_strand_barcodes.

Metagenome assembly, binning, and quality assessment

For the sediment metagenome from site LCB070, raw metagenomic reads were processed according to JGI's standard workflow, and quality controlled reads were assembled using SPAdes[47] 3.14.1 with options -m 2000 -k 33,55,77,99,127 and -meta. For the enrichment culture metagenome, Illumina reads were evaluated with FastQC v0.11.5 to determine best parameters before trimming (quality, linker, and adapter). Artifact and common contaminant

removal was done with rqcfilter2 (maxns=3, maq=3, minlen=51) followed by error correction with bbcms (mincount=2, hcf=0.6) from the BBTools suite v38.94[48]. Resulting reads were assembled with SPAdes v3.15.3 (-k 33,55,77,99,111 -meta –only-assembler) and coverage was determined by mapping the cleaned and corrected reads to the assembled sequences with bbmap (ambiguous=random). Assembled sequences ≥2,000 bp in length were binned with four programs: Maxbin v2.2.7[49], Concoct v1.0.0[50], Metabat v2.12.1 (with and without coverage)[51], and Autometa v1 (bacterial and archaeal modes, including the machine learning step)[52] followed by bin refinement with DAS_Tool v1.1.2[53], as previously described[26]. CheckM v1.1.3[54] was used to assess MAG completeness and redundancy.

Assembly of the circular genome of LCB70

A long-read assembly was created using nanopore reads with metaFlye (v. 2.8.2), specifying three polishing iterations[55]. This step produced a circular assembly of the LCB70 genome. Long-read polishing was done with Medaka (v. 1.5.0), consisting of mini_align, medaka_consensus, the model 941_min_hac_g507, and the medaka stitch commands. Following this, Polypolish[56] was used to polish the assembly three times with the Illumina reads. Finally, three additional rounds of polishing using the Illumina reads were carried out with Polca[57], producing a final polished assembly.

Amplicon sequencing and analysis

A 1 mL aliquot of culture was pelleted by centrifugation (16,000 x g; 5 minutes) and DNA from the cell pellet was extracted using the FastDNA Spin Kit for Soil (MP Biomedicals) following the manufacturer's guidelines. Archaeal and bacterial 16S rRNA genes were amplified with the Earth Microbiome Project primer set 515F and 806R[58,59], amplicon libraries were prepared as described previously[60], and sequencing was performed at the Molecular Research Core Facility at Idaho State University (Pocatello, ID) using an Illumina MiSeq platform with 2 x 250 bp paired end read chemistry. Reads were processed as described previously[60] with QIIME 2 (version 2020.2)[61]. Briefly, barcode sequences were removed with cutadapt and then reads were truncated (209 forward, 215 reverse). Reads were denoised, merged, and chimera-checked with DADA2[62] using default settings. Taxonomic assignment of amplicon sequence variants was done using the sklearn method and the Silva SSU database[39] release 132.

Phylogenetic analyses

The 16S rRNA sequences encoded in publicly available Methanomethylicia MAGs were aligned and masked against reference archaeal 16S rRNA sequences using SSU-ALIGN v0.1.1[63], which produced a final alignment of 1,376 positions. Maximum likelihood analysis was performed using FastTree v2.1.10 and default parameters.

A set of 33 single-copy marker proteins (Supplementary Table 3) were collected from Methanomethylicia MAGs and reference archaeal genomes. These markers were aligned with MUSCLE[64], trimmed with trimAL[65] using a 50% gap threshold, and concatenated to produce a final alignment of 7,118 positions. IQtree2 was used to reconstruct a maximum likelihood phylogenetic tree and ModelFinder[66] was used to select the best fit model with the additional

option --madd LG+C60,LG+C60+F+G,LG+C60+F+R. The best fit LG+F+R10 model was selected according to Bayesian inference criterion and branch support was evaluated with 1,000 ultrafast bootstraps and 1,000 iterations of the SH-like approximate-likelihood ratio test[67].

The McrA sequence of LCB70 was aligned against a set of publicly available reference sequences using MAFFT-linsi[68], trimmed with trimAL using a 50% gap threshold. A maximum likelihood phylogenetic tree was reconstructed using IQtree2, using the LG+C60+F+G model and 1,000 ultrafast bootstraps.

Sequences of catalytic subunits of group 4 [NiFe]-hydrogenases encoded by LCB70 were aligned against the HydDB reference sequences and reference FpoD/NuoD subunits. Additional Ehi sequences were collected through Blastp searches of the NCBI nr and IMG databases using the strain LCB70 sequence as a query. References were aligned with MAFFT-linsi and trimmed with trimAL using a 50% gap threshold, producing a final alignment of 365 residues. Maximum likelihood phylogenetic trees were constructed with IQtree2 with the model LG+C60+R+F and 1000 ultrafast bootstraps.

Annotation and reconstruction of metabolic potential

MAGs were annotated using Prokka v1.14.6[69] with both default and custom/in-house annotation databases. Refinement and confirmation of the initial annotation was done by submission of protein sequences to the NCBI conserved domain database[70] and HHpred[71] using default settings. Furthermore, the strain LCB70 genome was uploaded to the IMG/M database for annotation[72]. The catalytic subunits of [NiFe] hydrogenases were submitted to HydDB[73] for classification and further confirmed through phylogenetic analysis (above).

Chemical analyses of methane and methanol

During cultivation, subsamples of the headspace were taken with a gas tight syringe (Hamilton) and injected into 10 mL autosampler vials that had been sealed with grey chlorobutyl septa. Samples were taken from the autosampler vials and injected into a Shimadzu 2020-GC gas chromatograph equipped with a GS-CarbonPLOT column (30 m x 0.32 mm; 1.5 µm film thickness; Agilent) and a Rt-Q-BOND column (30 m x 0.32 mm; 1.5 µm film thickness; Restek) and using Helium as a carrier gas. The injector, column, and flame ionization detector (FID) were maintained at 200 °C, 50 °C, and 240 °C, respectively. Methane concentrations were calculated based on injection of a standard curve. For methanol quantification, liquid subsamples were taken with a needle and syringe. The liquid was cleared by centrifugation (16,000 x g; 5 minutes; 4 °C). Then, 400 µL of supernatant was placed in a sealed, gas-tight 10 mL vial and stored at -20 °C. For analysis, the liquid was heated to 80 °C for 5 minutes and then 500 µL of headspace was injected into the Shimadzu 2020-GC gas chromatograph. Methanol concentrations were calculated based on injection of a standard curve.

BONCAT-FISH and inhibition experiments

Experiments were carried out in 30 mL culture volumes in 60 mL serum bottles. A control bottle contained 10 mM BES inhibitor at the start of the experiment. After 10 days of growth one set of replicate cultures was spiked with 10 mM BES and the cultures were incubated for 48 hours, after which 100 µM of the amino acid analog *L*-homopropargylglycine (HPG) was

added to all cultures, except a no HPG control bottle. After HPG addition, the cultures were incubated for 24 hours, and subsamples were fixed in PFA for bioorthogonal non-canonical amino acid tagging and fluorescence in situ hybridization (BONCAT-FISH) analyses. The azide-alkyne click chemistry reaction was performed as described in Hatzenpichler *et al.* 2016[20] and used azide-labeled TexasRed (Click Chemistry Tools). Following the click chemistry reaction, DOPE-FISH was performed as described above with a 2xFAM labeled Msur657 probe.

Stable isotope tracing

For tracking the conversion of ^{13}C-MeOH to ^{13}C-CH4, active cultures were incubated in the presence of ^{12}C-MeOH or ^{13}C-MeOH under a 90% N_2, 10% CO_2 headspace. During the incubation, headspace samples were injected into a Shimadzu QP2020 NX GCMS equipped with a GS-CarbonPLOT column (30 m x 0.35 mm; 1.5 µm film thickness; Agilent) using the method described in Ai *et al.* 2013[74] and Helium as a carrier gas. The collection was run in Selected Ion Monitoring mode and peak areas corresponding to m/z of 16 for $^{12}CH_4$, 17 for $^{13}CH_4$, 44 for $^{12}CO_2$, and 45 for $^{13}CO_2$ were used for quantification.

Habitat distribution

The 16S rRNA gene sequence for strain LCB070 was submitted to the IMNGS webserver[75] to search the NCBI Sequence Read Archive (SRA) for sequences with a sequence similarity cutoff of 97% and a minimum size of 200 bp. Metadata on the sample collection source was collected from each SRA sample that had sequence hits.

Plunge freezing for Cryo-electron tomography

An active methanogenic enrichment culture grown at 64 °C was used for plunge freezing. In order to concentrate the biomass prior to freezing, 500 µL of the enrichment culture were centrifuged at 16,000 x g for 10 min at 20°C and the resulting pellet was resuspended in 100 µL of the supernatant. Then, the sample was mixed with Protein A-conjugated 10 nm colloidal gold. All the above steps were performed in an anoxic chamber. 3.5 µL of the enrichment culture were then applied to glow-discharged copper EM grids (R2/1, Quantifoil), automatically blotted for 4, 8 or 10 seconds and plunged into liquid ethane using a Vitrobot Mark IV (Thermo Fisher Scientific)[76]. The plunge frozen grids were clipped into autoloader grids, stored in liquid nitrogen, and shipped to Zurich (Switzerland).

Cryo-electron tomography

A cryo-electron tomography dataset was collected on a Titan Krios G4 EM (ThermoFisher) operating at 300 kV and equipped with BioContinuum imaging energy filter (slit width 20 eV) and a K3 Summit camera (Gatan). The tilt series were collected at a magnification of 19,500 (effective pixel size 4.51 Å) with a defocus of -8 µm using a bidirectional scheme from -60° to +60° in 2° incremental steps using SerialEM[77]. The total dose of a tilt series was 165 to 180e^- /Å^2.

Tomogram reconstruction and segmentation

LCB070 cells were identified by their unique morphology (via FISH), their high relative abundance in the culture, and their S-layer. Three dimensional (3D) tomograms were generated using gold fiducial alignment and weighted-back projection reconstruction in the IMOD software package[78,79]. To increase contrast, some tomograms were filtered using tom-deconv deconvolution filter[80]. The 3D segmentations of tomograms and videos were generated using IMOD or UCSF Chimera X[81].

Protologue

Methanosuratincolia classis nov.

Me.tha.no.su.rat.in.co'li.a. N.L. masc. n. *Methanosuratincola*, type genus of the class; -*ia*, ending to designate a class; N.L. neut. pl. n. *Methanosuratincolia*, the *Methanosuratincola* class. The description is the same as for *Methanosuratincola* gen. nov.

Methanosuratincolales ord. nov.

Me.tha.no.su.rat.in.co.la'les. N.L. masc. n. *Methanosuratincola*, type genus of the order; -*ales*, ending to designate an order; N.L. fem. pl. n. *Methanosuratincolales*, the *Methanosuratincola* order. The description is the same as for *Methanosuratincola* gen. nov.

Methanosuratincolaceae fam. nov.

Me.tha.no.su.rat.in.co.la'ce.ae N.L. masc. n. *Methanosuratincola*, type genus of the family; -*aceae*, ending to designate a family; N.L. fem. pl. n. *Methanosuratincolaceae*, the *Methanosuratincola* family. The description is the same as for *Methanosuratincola* gen. nov.

Methanosuratincola gen. nov.

Me.tha.no.su.rat.in'co.la. N.L. pref. *methano*-, pertaining to methane; L. masc. or fem. n. *incola*, inhabitant, dweller; N.L. masc. n. *Methanosuratincola*, methane organism inhabiting the Surat Basin, where this lineage was discovered[6]. The type species is *Methanosuratincola yellowstonensis* sp. nov. Following the suggestion by Oren *et al*.[19] we propose the corrected genus name *Methanosuratincola* to refer to this lineage that was originally discovered via metagenomics by Vanwonterghem *et al*.[6].

Methanosuratincola yellowstonensis sp. nov.

yel.low.ston.en'sis N.L. masc. adj. *yellowstonensis*, from Yellowstone National Park. This archaeon was cultured from an unnamed hot spring in Yellowstone National Park that we identified as feature LCB070 in a recent survey[16]. The archaeon is a thermophilic methyl-reducing hydrogenotrophic methanogen growing as coccoid cells with a diameter of 845 ± 163 nm.

Reporting summary

Further information on research design is available in the Nature Portfolio Reporting Summary linked to this article.

Data availability

The LCB70 enrichment culture metagenomic (raw reads and MAGs) and amplicon data are deposited under NCBI BioProject ID PRJNA916083. The LCB070 hot spring metagenome is publicly available on the IMG database under the taxon ID 3300043544 and the strain LCB70 genome under taxon ID 3300059795. Representative cryo-tomograms will be deposited at EMDB/EMPIAR with accession numbers XYZ.

References

38 Brandis, A. & Thauer, R. K. Growth of Desulfovibrio species on hydrogen and sulphate as sole energy source. *Microbiology* **126**, 249-252 (1981).

39 Quast, C. *et al.* The SILVA ribosomal RNA gene database project: improved data processing and web-based tools. *Nucleic acids research* **41**, D590-D596 (2012).

40 Ludwig, W. *et al.* ARB: a software environment for sequence data. *Nucleic acids research* **32**, 1363-1371 (2004).

41 Stoecker, K., Dorninger, C., Daims, H. & Wagner, M. Double labeling of oligonucleotide probes for fluorescence in situ hybridization (DOPE-FISH) improves signal intensity and increases rRNA accessibility. *Applied and environmental microbiology* **76**, 922-926 (2010).

42 Stahl, D. A. Development and application of nucleic acid probes. *Nucleic acid techniques in bacterial systematics*, 205-248 (1991).

43 Wallner, G., Amann, R. & Beisker, W. Optimizing fluorescent in situ hybridization with rRNA-targeted oligonucleotide probes for flow cytometric identification of microorganisms. *Cytometry: The Journal of the International Society for Analytical Cytology* **14**, 136-143 (1993).

44 Daims, H. Use of fluorescence in situ hybridization and the daime image analysis program for the cultivation-independent quantification of microorganisms in environmental and medical samples. *Cold Spring Harbor Protocols* **2009**, pdb. prot5253 (2009).

45 Daims, H., Lücker, S. & Wagner, M. Daime, a novel image analysis program for microbial ecology and biofilm research. *Environmental microbiology* **8**, 200-213 (2006).

46 Zhou, J., Bruns, M. A. & Tiedje, J. M. DNA recovery from soils of diverse composition. *Appl. Environ. Microbiol.* **62**, 316-322 (1996).

47 Nurk, S., Meleshko, D., Korobeynikov, A. & Pevzner, P. A. metaSPAdes: a new versatile metagenomic assembler. *Genome research* **27**, 824-834 (2017).

48 Bushnell, B. BBMap: a fast, accurate, splice-aware aligner. (Lawrence Berkeley National Lab.(LBNL), Berkeley, CA (United States), 2014).

49 Wu, Y.-W., Tang, Y.-H., Tringe, S. G., Simmons, B. A. & Singer, S. W. MaxBin: an automated binning method to recover individual genomes from metagenomes using an expectation-maximization algorithm. *Microbiome* **2**, 1-18 (2014).

50 Alneberg, J. *et al.* Binning metagenomic contigs by coverage and composition. *Nature methods* **11**, 1144-1146 (2014).

51 Kang, D. D. *et al.* MetaBAT 2: an adaptive binning algorithm for robust and efficient genome reconstruction from metagenome assemblies. *PeerJ* **7**, e7359 (2019).
52 Miller, I. J. *et al.* Autometa: automated extraction of microbial genomes from individual shotgun metagenomes. *Nucleic acids research* **47**, e57-e57 (2019).
53 Sieber, C. M. *et al.* Recovery of genomes from metagenomes via a dereplication, aggregation and scoring strategy. *Nature microbiology* **3**, 836-843 (2018).
54 Parks, D. H., Imelfort, M., Skennerton, C. T., Hugenholtz, P. & Tyson, G. W. CheckM: assessing the quality of microbial genomes recovered from isolates, single cells, and metagenomes. *Genome research* **25**, 1043-1055 (2015).
55 Kolmogorov, M. *et al.* metaFlye: scalable long-read metagenome assembly using repeat graphs. *Nature Methods* **17**, 1103-1110 (2020).
56 Wick, R. R. & Holt, K. E. Polypolish: Short-read polishing of long-read bacterial genome assemblies. *PLoS computational biology* **18**, e1009802 (2022).
57 Zimin, A. V. & Salzberg, S. L. The genome polishing tool POLCA makes fast and accurate corrections in genome assemblies. *PLoS computational biology* **16**, e1007981 (2020).
58 Apprill, A., McNally, S., Parsons, R. & Weber, L. Minor revision to V4 region SSU rRNA 806R gene primer greatly increases detection of SAR11 bacterioplankton. *Aquatic Microbial Ecology* **75**, 129-137 (2015).
59 Parada, A. E., Needham, D. M. & Fuhrman, J. A. Every base matters: assessing small subunit rRNA primers for marine microbiomes with mock communities, time series and global field samples. *Environmental microbiology* **18**, 1403-1414 (2016).
60 Reichart, N. J. *et al.* Activity-based cell sorting reveals responses of uncultured archaea and bacteria to substrate amendment. *The ISME journal* **14**, 2851-2861 (2020).
61 Bolyen, E. *et al.* Reproducible, interactive, scalable and extensible microbiome data science using QIIME 2. *Nature biotechnology* **37**, 852-857 (2019).
62 Callahan, B. J. *et al.* DADA2: High-resolution sample inference from Illumina amplicon data. *Nature methods* **13**, 581-583 (2016).
63 Nawrocki, E. P., Kolbe, D. L. & Eddy, S. R. Infernal 1.0: inference of RNA alignments. *Bioinformatics* **25**, 1335-1337 (2009).
64 Edgar, R. C. MUSCLE: multiple sequence alignment with high accuracy and high throughput. *Nucleic acids research* **32**, 1792-1797 (2004).
65 Capella-Gutiérrez, S., Silla-Martínez, J. M. & Gabaldón, T. trimAl: a tool for automated alignment trimming in large-scale phylogenetic analyses. *Bioinformatics* **25**, 1972-1973 (2009).
66 Kalyaanamoorthy, S., Minh, B. Q., Wong, T. K., Von Haeseler, A. & Jermiin, L. S. ModelFinder: fast model selection for accurate phylogenetic estimates. *Nature methods* **14**, 587-589 (2017).
67 Guindon, S. *et al.* New algorithms and methods to estimate maximum-likelihood phylogenies: assessing the performance of PhyML 3.0. *Systematic biology* **59**, 307-321 (2010).
68 Katoh, K. & Standley, D. M. MAFFT multiple sequence alignment software version 7: improvements in performance and usability. *Molecular biology and evolution* **30**, 772-780 (2013).
69 Seemann, T. Prokka: rapid prokaryotic genome annotation. *Bioinformatics* **30**, 2068-2069 (2014).
70 Lu, S. *et al.* CDD/SPARCLE: the conserved domain database in 2020. *Nucleic acids research* **48**, D265-D268 (2020).
71 Zimmermann, L. *et al.* A completely reimplemented MPI bioinformatics toolkit with a new HHpred server at its core. *Journal of molecular biology* **430**, 2237-2243 (2018).

72 Chen, I.-M. A. *et al.* IMG/M v. 5.0: an integrated data management and comparative analysis system for microbial genomes and microbiomes. *Nucleic acids research* **47**, D666-D677 (2019).
73 Søndergaard, D., Pedersen, C. N. & Greening, C. HydDB: a web tool for hydrogenase classification and analysis. *Scientific reports* **6**, 1-8 (2016).
74 Ai, G., Zhu, J., Dong, X. & Sun, T. Simultaneous characterization of methane and carbon dioxide produced by cultured methanogens using gas chromatography/isotope ratio mass spectrometry and gas chromatography/mass spectrometry. *Rapid Communications in Mass Spectrometry* **27**, 1935-1944 (2013).
75 Lagkouvardos, I. *et al.* IMNGS: a comprehensive open resource of processed 16S rRNA microbial profiles for ecology and diversity studies. *Scientific reports* **6**, 1-9 (2016).
76 Iancu, C. V. *et al.* Electron cryotomography sample preparation using the Vitrobot. *Nature protocols* **1**, 2813-2819 (2006).
77 Mastronarde, D. N. Automated electron microscope tomography using robust prediction of specimen movements. *Journal of structural biology* **152**, 36-51 (2005).
78 Kremer, J. R., Mastronarde, D. N. & McIntosh, J. R. Computer visualization of three-dimensional image data using IMOD. *Journal of structural biology* **116**, 71-76 (1996).
79 Mastronarde, D. Correction for non-perpendicularity of beam and tilt axis in tomographic reconstructions with the IMOD package. *Journal of microscopy* **230**, 212-217 (2008).
80 Tegunov, D. & Cramer, P. Real-time cryo-electron microscopy data preprocessing with Warp. *Nature methods* **16**, 1146-1152 (2019).
81 Pettersen, E. F. *et al.* UCSF ChimeraX: Structure visualization for researchers, educators, and developers. *Protein Science* **30**, 70-82 (2021).

Acknowledgements

This study was funded through a NASA Exobiology program award (80NSSC19K1633) with minor support from the Simons and the Gordon and Betty Moore Foundations (award 737750). M.P. was supported by the European Research Council (CoG 101000232). A portion of this research was performed under the Community Sciences Program (proposal 10.46936/10.25585/60008108) and used resources at the DOE Joint Genome Institute (https://ror.org/04xm1d337), which is a DOE Office of Science User Facility operated under Contract No. DE-AC02-05CH11231. We thank the US National Park Service for permitting work in YNP under permit number YELL-SCI-8010 and ScopeM for instrument access at ETH Zürich. We thank Grayson Chadwick (UC Berkeley) for discussions on archaeal cell biology and physiology, Alex Charbonneau (MSU) and Anastasiia Kokhanovska (ETH Zurich) for help with cryoET, Mackenzie Lynes (MSU) for discussions that informed field sampling efforts, and Marike Palmer (UN Las Vegas) for valuable input on taxonomy and systematics.

Author contributions

A.J.K. and R.H. developed the research project. A.J.K., V.K., and R.H. designed experiments. A.J.K., V.K., and Z.J.J. conducted field sampling. A.J.K. conducted cultivation, BONCAT, SIP, and FISH experiments, performed culture DNA extractions, and phylogenetic analysis of

hydrogenases. V.K. extracted DNA from LCB070 sediment, advised on cultivation, and performed phylogenetic analysis of MCR sequences. Z.J.J. and A.J.K analyzed metagenomic data and performed phylogenetic analysis of genomes. A.J.K performed the metabolic reconstruction with input from Z.J.J. and V.K. N.P. collected and analyzed cryoET data. N.P. and M.P. analyzed cryoET data, with input from A.J.K and R.H. R.H. was responsible for funding and supervision of the project. A.J.K. and R.H. wrote the manuscript with input from all authors.

Competing interests

The authors declare no competing interests.

Extended figures

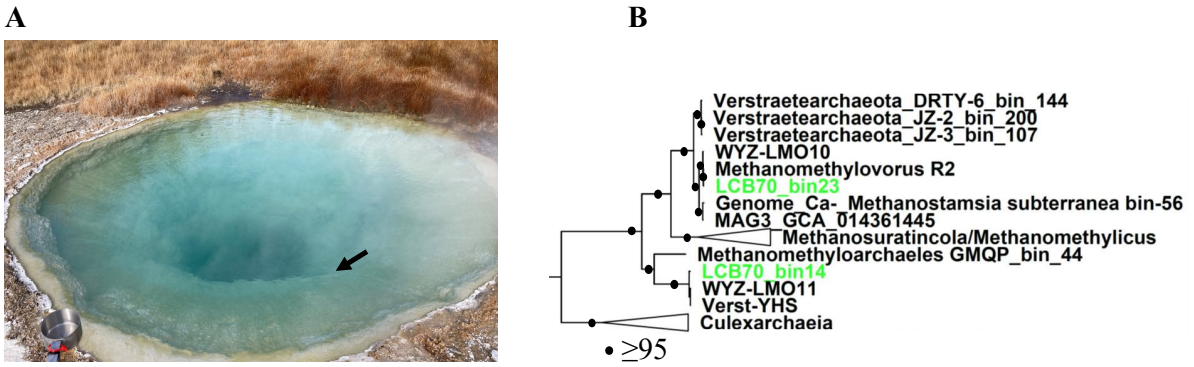

Extended Data Figure 1. Image of hot spring LCB070 and diversity of Methanomethylicia MAGs recovered from the hot spring sediment metagenome. A. Hot spring LCB070 in Yellowstone National Park. The arrow indicates the location where sediment samples were taken. **B.** Phylogenomic tree of Methanomethylicia, rooted with MAGs from the closely related lineage, Culexarchaeia[26]. MAGs recovered from the sediment metagenome are highlighted in green.

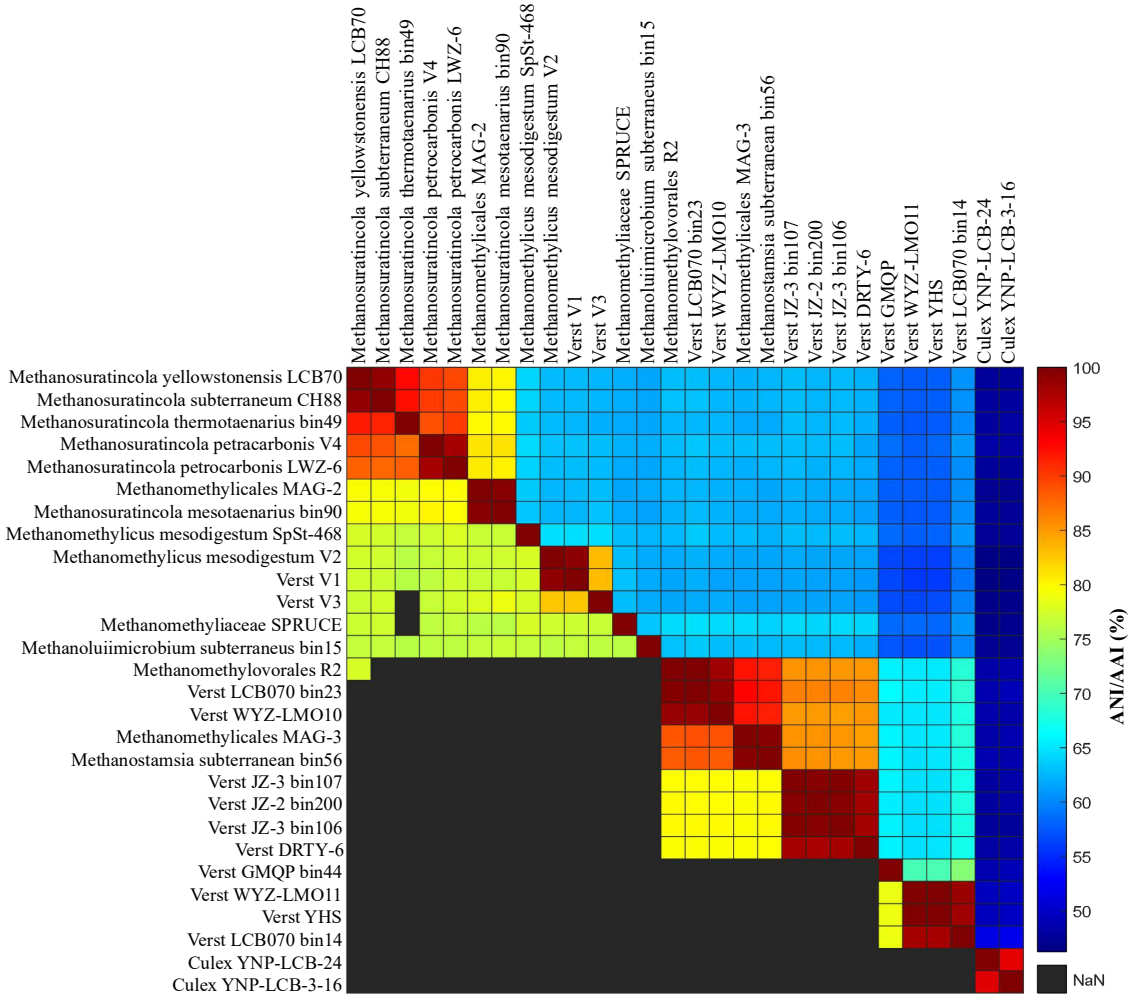

827

828 **Extended Data Figure 2. Pairwise comparison of Methanomethylicia MAG sequence**
829 **identities.** Pairwise average amino acid identity (AAI, top) and average nucleotide identity
830 (ANI, bottom) values (in %) were calculated by compareM and FastANI, respectively. Two
831 MAGs from the closely related class Culexarchaeia[26], were used as an outgroup. The two
832 Verstraetearchaeota-affiliated MAGs reconstructed from the original hot spring (LCB070
833 bin14 and bin 23) have less than 75% ANI similarity to the genome of *Ca.* M. yellowstonensis
834 strain LCB70.

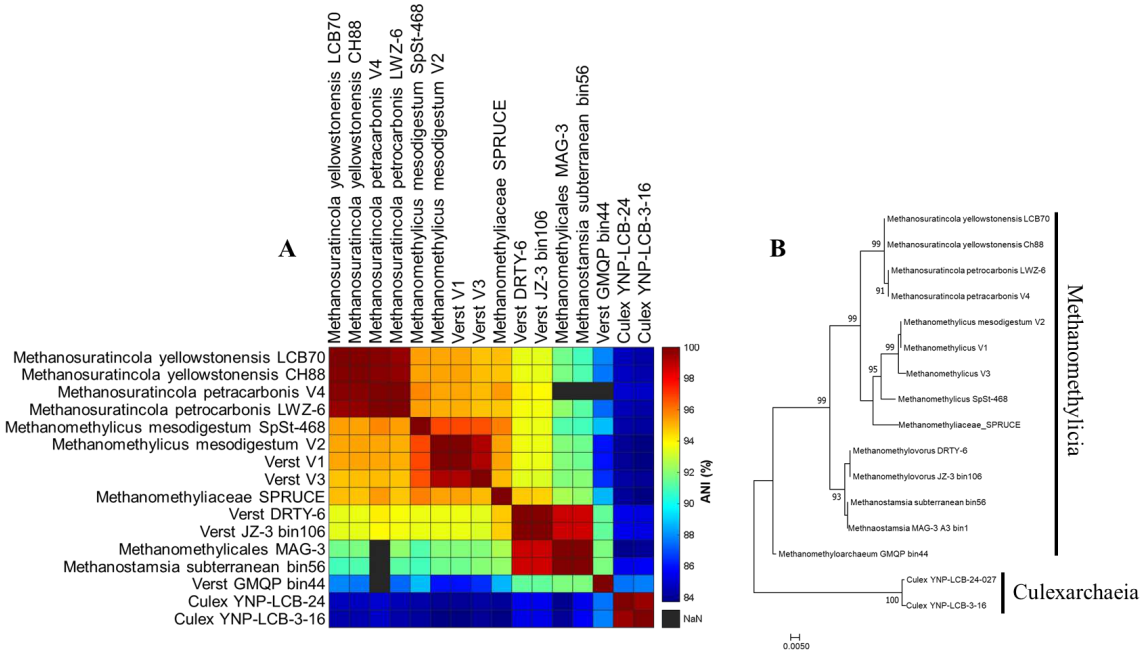

835

836 **Extended Data Figure 3. Pairwise comparison of 16S rRNA sequence identity and**
837 **phylogeny. A.** Pairwise percent sequence identity was calculated with BLASTn. **B**. Maximum
838 likelihood phylogenetic tree of full length and partial 16S rRNA genes encoded in strain
839 LCB70 and representative Methanomethylicia MAGs. Numbers at the nodes indicate bootstrap
840 support, only values above 90 are shown.

841

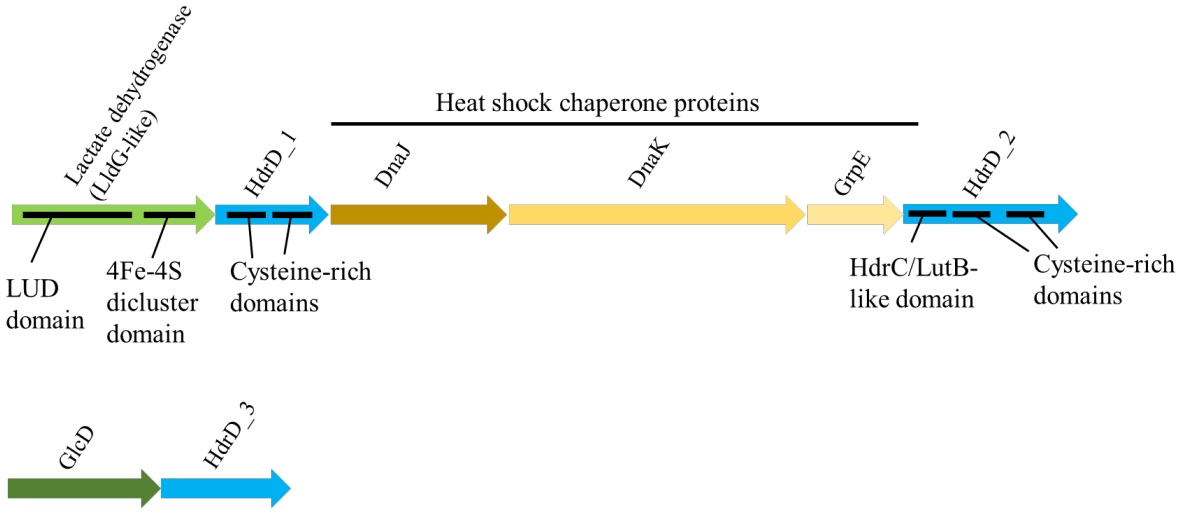

842

843 **Extended Data Figure 4. Genomic context of putative lactate dehydrogenase and**
844 **heterodisulfide reductase (HdrD) subunits.** Sequences are indicated by arrows and distinct
845 domains within the protein coding sequence are indicated by black bars. LUD, Lactate
846 Utilization Domain.

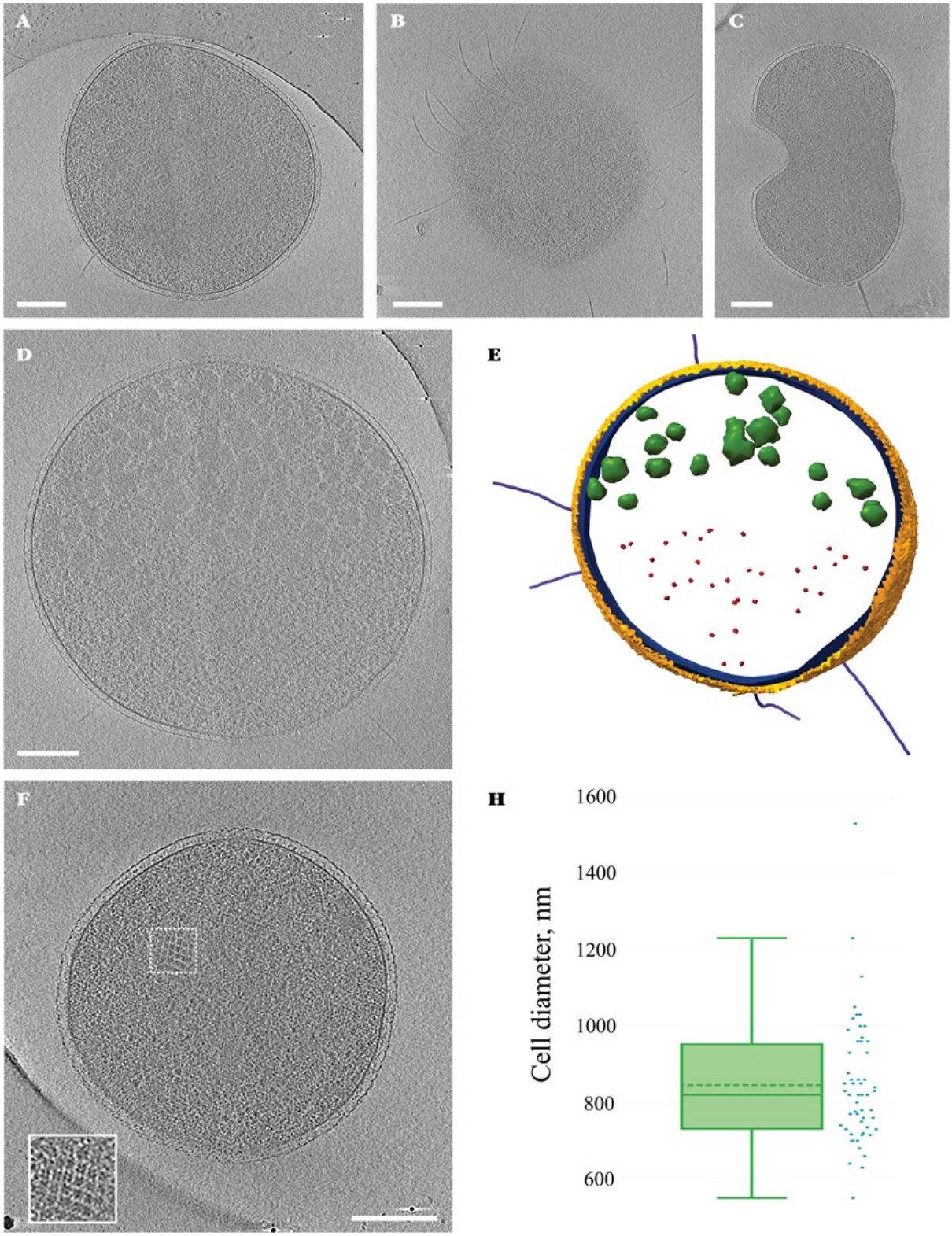

Extended Data Figure 5. Cell biology of strain LCB70. A, B. Two tomographic slices of an archaellated LCB70 cell. **C.** Example of a dividing LCB70 cell. **D, E.** A tomographic slice and the corresponding model of a cell with putative storage granules. S-layer colored in yellow, inner membrane in blue, ribosomes in red and storage granules in green. **F.** A LCB70 cell with unidentified filamentous structures. A zoomed-in view is shown in the inset. **G.** Boxplot representing the variation in LCB70 cell diameters (n = 56). Dashed line represents the average cell diameter. For all tomographic slices the scale bar is 200 nm.

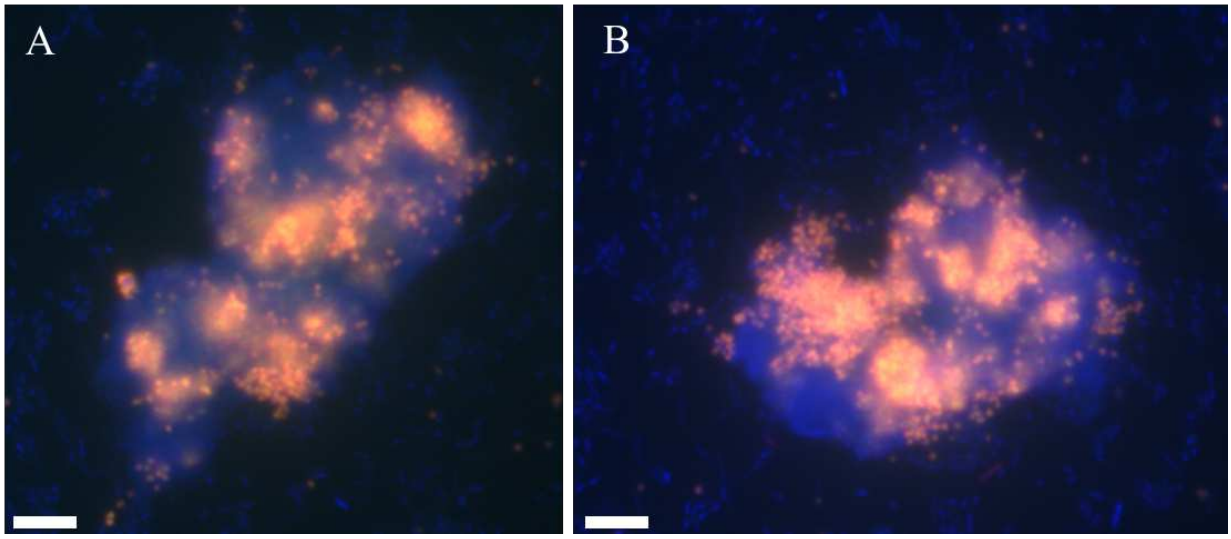

Extended Data Figure 6. A, B Two examples of cell aggregates in the culture. Cells are stained with the general nucleic acid stain DAPI (blue), and the Methanomethylicia-specific FISH probe Msur657 (green), and the general archaeal probe Arch915 (red). Strain LCB70 cells bind to both the Msur657 and Arch915 probes, appearing orange. Scale bars, 5µm.

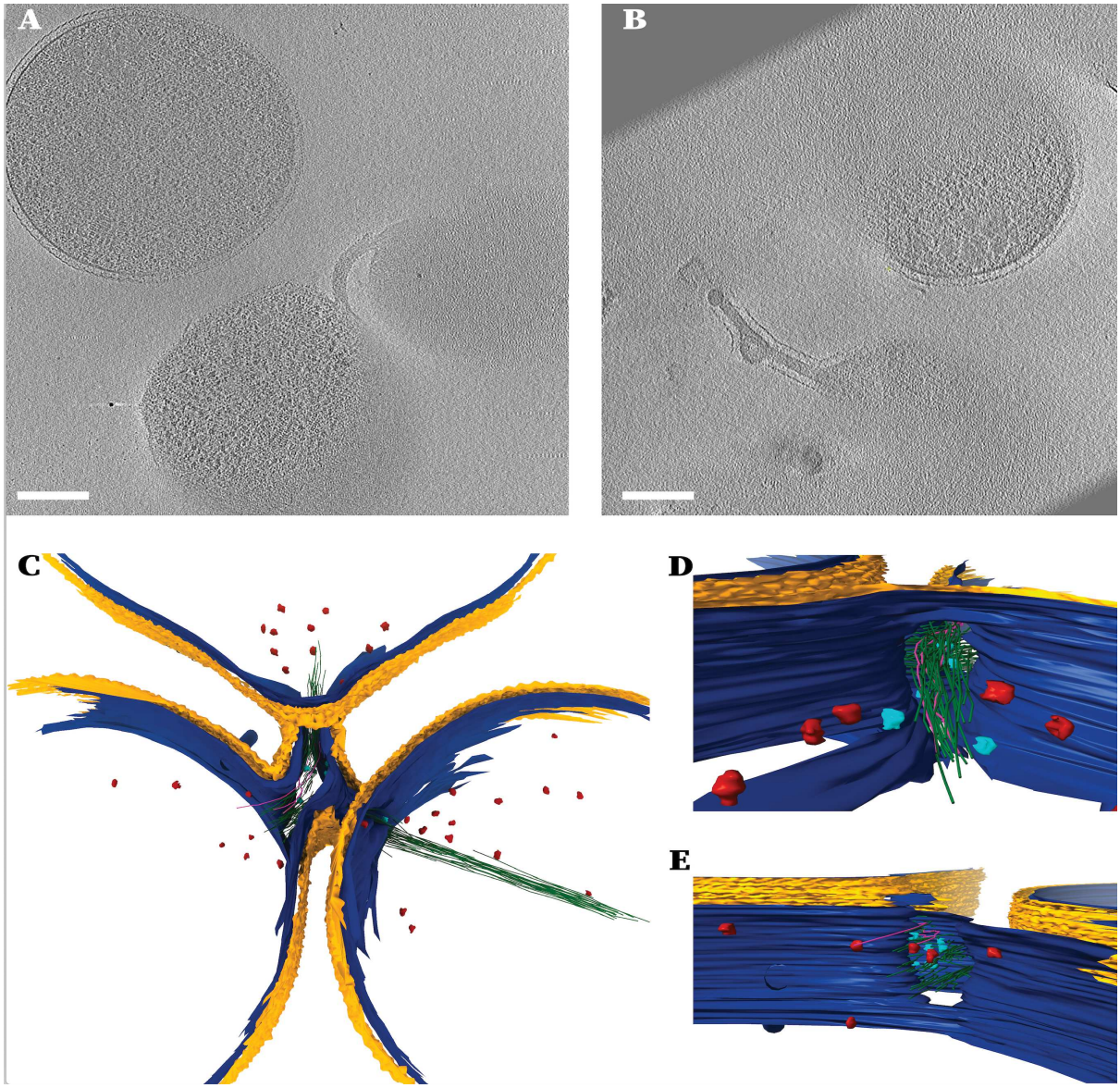

Extended Data Figure 7. Cell-cell connections between LCB70 cells. A, B. Two examples of interactions between LCB70 cells. Cell-cell bridges that are uncovered (panel A) or covered by a S-layer (panel B) formed from the inner membrane connecting two cells. **C-E**. A model of a junction between the three cells shown in Fig. 4C. The zoomed in views of the cell junction (panel D and E) show filaments and two putative ribosomal populations: inside the junction (cyan) and in cytoplasm (red). S-layer colored in yellow, cytoplasmic membrane in blue. For all tomographic slices the scale bar is 200 nm.

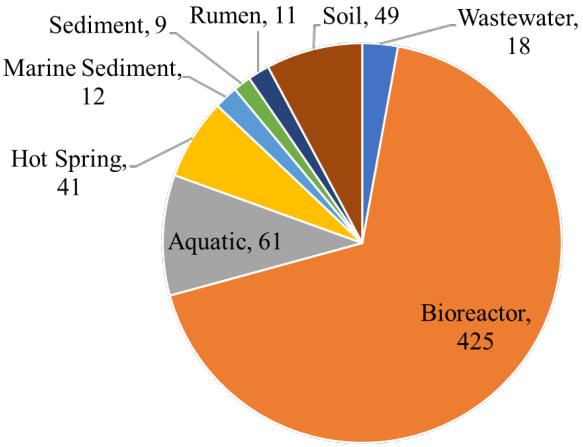

868

869 **Extended Data Figure 8. Habitat distribution of *Ca.* M. yellowstonensis LCB70 and**
870 **related species.** Sequences were found by searching the NCBI SRA database using the IMNGS
871 webserver with default settings. Graph is based on presence of 16S rRNA gene sequences with
872 >97% sequence identity to strain LCB70 across 626 public samples.

Supplementary Tables 1-4. See separate Excel file.

Supplementary Table 1. Summary of the *Ca.* M. yellowstonensis strain LCB70 genome and Metagenome Assembled Genomes (MAGs) recovered from the enrichment metagenome.

Supplementary Table 2. List of annotated genes in the strain LCB70 genome used to build Figure 3. Annotations were generated by the IMG/M annotation pipeline.

Supplementary Table 3. List of single copy marker genes used in phylogenomic analyses.

Supplementary Table 4. FISH probes used in this study.

Supplementary Movie 1. The movie shows tomographic slices through a *Ca.* Methanosuratincola yellowstonensis LCB70 cell followed by the corresponding 3D model representation (same dataset as shown in Figure 4AB). In the 3D model the colors refer to: S-layer (yellow), cytoplasmic membrane (blue), putative ribosomes (red), archaella (purple), viruses (cyan), chemotaxis receptor arrays (pink), and unidentified filamentous structures (green).

Supplementary Files

This is a list of supplementary files associated with this preprint. Click to download.

- Supplementarytables14.xlsx
- ExtendedDataMovie1.mp4